



### **Geophysical Research Letters**°



#### **RESEARCH LETTER**

10.1029/2023GL106004

#### **Key Points:**

- Changes in water availability under climate change scenarios are evaluated
- Sub-humid basins are most often impacted
- Vulnerability increase is large due to increase in Potential Evapotranspiration

#### **Supporting Information:**

Supporting Information may be found in the online version of this article.

#### Correspondence to:

F. T. Wolkeba, fwolkeba@crimson.ua.edu

#### Citation:

Wolkeba, F. T., Kumar, M., & Mekonnen, M. M. (2023). Examining the water scarcity vulnerability in US river basins due to changing climate. *Geophysical Research Letters*, *50*, e2023GL106004. https://doi.org/10.1029/2023GL106004

Received 23 AUG 2023 Accepted 26 NOV 2023

# © 2023. The Authors. This is an open access article under the terms of the Creative Commons Attribution License, which permits use, distribution and reproduction in any medium, provided the original work is

properly cited.

## **Examining the Water Scarcity Vulnerability in US River Basins Due To Changing Climate**

Fitsume T. Wolkeba<sup>1</sup>, Mukesh Kumar<sup>1</sup>, and Mesfin M. Mekonnen<sup>1</sup>

<sup>1</sup>Department of Civil, Construction, and Environmental Engineering, University of Alabama, Tuscaloosa, AL, USA

**Abstract** Accurate assessment of changes in water availability with changing climate is vital for effective mitigation and adaptation. In this research, we employ a parsimonious Budyko curve method to evaluate changes in water availability under low- (SSP126) and high-emission (SSP585) scenarios for 331 river basins in the contiguous United States. We also assess the relative role of changes in precipitation ( $\Delta P$ ) and potential evapotranspiration ( $\Delta PET$ ) with changing climate on the increase in water availability vulnerability. Results highlight that around 43% (28%) of basins are projected to experience increased vulnerability to changing climate in high-emission (low-emission) scenarios. Sub-humid basins are most often impacted, while arid and semi-arid basins exhibit lower sensitivity to changes. Intriguingly,  $\Delta PET$  emerges as the dominant control on vulnerability, surpassing  $\Delta P$ , particularly under SSP585 scenario. The analysis prompts water managers to focus on long-term mitigation planning and scientists to further constraint climate and water budget forecasts in affected basins.

Plain Language Summary Assessment of changes in water availability because of the changing climate is useful for mitigation and adaptation planning. In this study, water availability change in river basins in the contiguous United States is assessed. Which basins will become more vulnerable in terms of reduced water availability in the future climate and how the vulnerability changes within different aridity zones is studied. The study presents a novel methodology to assess and quantify whether the changes in potential evapotranspiration or precipitation are the main driver of future water vulnerability. We find that vulnerability increase due to an increase in potential evapotranspiration to be large. From the different aridity zones, sub-humid basins are projected to most often experience an increase in vulnerability.

#### 1. Introduction

With changing climate, water availability is changing all over the world (Guan et al., 2022; Konapala et al., 2020; Koutroulis et al., 2019; Mekonnen & Hoekstra, 2016; Pokhrel et al., 2021). The change may be an increase or a decrease in overall water availability. Before creating bespoke mitigation, management, and/or adaptation plans at watershed to river basin scales, it is critical to first map the extent and trend of these impacts. This is especially challenging as the impacts on water availability depend on complex interactions between multiple hydrological processes within a region (Ravazzani et al., 2015; Viola et al., 2021; Weiskel et al., 2007). Over the years, numerous process-based models (Kollet & Maxwell, 2006; Kumar et al., 2009; VanderKwaak & Loague, 2001) have been developed to study water availability under a changing climate. However, the limitation to such approaches is the unavailability of good quality observation data to parameterize the participating hydrological process (Telteu et al., 2021; Teshome et al., 2019; Zhang et al., 2004). In addition, many of the model parameters, such as vegetation properties are expected to change in a changing climate (Bouaziz et al., 2022), leading to added uncertainty in future water availability predictions. Although significant advances have been made in models of vegetation dynamics, large uncertainties remain (Fisher et al., 2018; Koyen et al., 2020; Martens et al., 2021). In this study, we use an alternative approach based on a parsimonious Budyko curve-based method, which implicitly accounts for the co-evolution of vegetation properties (Gan et al., 2021), to predict changes in water availability in 331 river basins in the contiguous US (CONUS).

Budyko curves can be used to assess water availability, and potential changes in it, with changing climate and land cover (Xu et al., 2014). Teng et al. (2012) demonstrated that the framework can perform comparable to process-based models in studying climate change impacts. The method has been used globally. For example, Singh and Kumar (2015) used a bottom-up probabilistic Budyko analysis to study water availability in India. Gunkel and Lange (2017) used the output of the hydrological model, global climate products, and the Budyko

WOLKEBA ET AL. 1 of 10

curve to study water scarcity in the data-scarce Lower Jordan River basin. Guan et al. (2021) used Budyko framework to estimate future projections of runoff in 10 river basins across China. Carmona et al. (2014) used the Budyko framework on 190 Model Parameter Estimation Project (MOPEX) catchments across the CONUS to estimate water availability, and reported spatial and temporal space-time symmetry of annual water balances. Greve et al. (2015) introduced a probabilistic Budyko framework to evaluate the predictability of water availability across various catchment characteristics. Gudmundsson et al. (2016) extended this framework to study the sensitivity of water availability to changes in aridity index. In a similar study, Berghuijs et al. (2017) used Budyko curve to study the sensitivity of runoff to changes in precipitation, PET, and other variables. In fact, numerous other studies have also employed the Budyko curve to assess the impact of land cover and climate changes on water availability (Abatzoglou, 2013; Abera et al., 2019; Greve et al., 2018; Li & Quiring, 2022). Although the studies noted above, and many more, have used Budyko curve to study water availability sensitivity and inter-annual variations in water budget components, an urgent question that remains unanswered is which river basins will become more vulnerable in terms of water availability in the future climate and how this vulnerability is changing within different aridity zones. Furthermore, it is still unknown whether the basins becoming vulnerable, is it contributed largely by changes in precipitation or potential evapotranspiration. This study addresses the two aforementioned questions by estimating climate change-induced vulnerability to water availability over 331 Hydrologic Unit Code-06 (HUC06) basins (Berelson et al., 2004) in the CONUS using the Budyko framework.

#### 2. Materials and Methods

#### 2.1. Budyko Framework

The Budyko curve, developed by Budyko (1961) for basins greater than 1,000 km², indicates the long-term partitioning of precipitation into evapotranspiration in a river basin as a function of the aridity index. It has been used to simulate long-term ET/P based on PET/P, where P is precipitation, ET is evapotranspiration and PET is potential evapotranspiration. Since its first development, many derivations of the curve have also been developed (Fu, 1981; L. Zhang et al., 2001; Pike, 1964; Schreiber, 1904). Fu's derivation (Fu, 1981; Zhang et al., 2004) is a popular one-parameter relationship analytically derived from the basic Budyko relationship. This study uses Fu's derivation (Equation 1) to simulate evaporation based on potential evapotranspiration.

$$\frac{ET}{P} = 1 + \frac{PET}{P} - \left(1 + \left(\frac{PET}{P}\right)^{\omega}\right)^{\frac{1}{\omega}}$$
 (1)

The Fu parameter  $\omega$  captures the influence of non-climatic factors such as soil, topography, and vegetation properties on basin water partitioning. Uncertainty in estimating  $\omega$  may adversely affect the predictability of water availability (Budyko, 1961; Greve et al., 2015; Gunkel & Lange, 2017; Guo et al., 2019; Singh & Kumar, 2015; Wang & Tang, 2014; Zhang et al., 2004). Here Fu's parameter  $\omega$  is calibrated using basin-aggregated long-term (2001–2022) average annual PET and ET from Moderate Resolution Imaging Spectroradiometer Version 6 Evapotranspiration/Latent Heat Flux product (MODIS), and precipitation from North American Land Data Assimilation System-phase 2 (NLDAS-2). To calibrate  $\omega$ , a nonlinear objective function (Equation 2) that minimizes root mean square error (RMSE) between Budyko-estimated actual ET and ET from MODIS is used.

RMSE = 
$$\sqrt{\frac{\sum (y_{1i} - y_{2i})^2}{n}}$$
 (2)

where, 
$$y_1 = 1 + \frac{PET}{P} - \left(1 + \left(\frac{PET}{P}\right)^{\omega}\right)^{\frac{1}{\omega}}$$
 and  $y_2 = \frac{ET}{P}$ 

It is to be noted that the scope of this study is solely to evaluate changes in water budget due to alterations in the ecohydrological response of river basins due to changes in climate. We do not account for the impacts of alterations in human water consumption and anthropogenically influenced land cover. That would necessitate dynamic modeling of  $\omega$  (Li & Quiring, 2022).

WOLKEBA ET AL. 2 of 10

9448007, 2023, 24, Downloaded from https://agupubs

com/doi/10.1029/2023GL106004, Wiley Online Library on [13/01/2024]. See the Terms and Conditi

#### 2.2. Evaluation of P and PET for the Future Period (2081–2100)

First, an average percentage change in precipitation (P) and potential evapotranspiration (PET) between 2015–2034 and 2081–2100 is evaluated. It is to be noted that 2015–2034 is the closest period to the base period during which projected data from Inter-Sectoral Impact Model Intercomparison Project (ISIMIP) is available. Percentage change in P and PET between the two periods is then used to obtain their future projections by accounting for the fractional change to P and PET respectively. Given that the Budyko method implicitly accounts for the coevolution of vegetation (Gan et al., 2021) with changing climate, the approach used here provides a parsimonious and computationally efficient means to estimate ET in a future climate. Notably, unlike the land surface models that are often used for prediction of ET and other water fluxes under a future climate, this approach is not vexed with parametrization challenges.

#### 2.3. Assessment of Water Availability and Basin's Vulnerability in a Changing Climate

Long-term water availability (WA), also called a renewable water resource, can be estimated as precipitation minus actual evapotranspiration (EU, 2015; Gunkel & Lange, 2017; Singh & Kumar, 2015).

$$WA = P - ET \tag{3}$$

Given that with changing climate, hydrologically, the river basin is expected to still fall on the same Budyko curve (Wang & Hejazi, 2011), Equation 1 can be used to estimate ET in the future period using projected estimates of P and PET (as derived in Section 2.2). Here we use the vulnerability Index (VI) as defined in Singh and Kumar (2015) to track the changes in WA to changes in PET and P due to changing climate.

$$VI = \frac{\Delta WA}{WA} \times 100 = \frac{WA_{Projetced} - WA_{Base Year}}{WA_{Base Year}} \times 100$$
 (4)

Negative values of VI indicate areas getting more vulnerable or with less available water, while positive values indicate areas having more water availability.

#### 2.4. Assessment of the Relative Role of Hydroclimatological Controls on VI

Given that negative  $\Delta P$  (= $P_{Projected} - P_{BaseYear}$ ) and positive  $\Delta PET$  (= $PET_{Projected} - PET_{BaseYear}$ ) enhances water vulnerability, basins experiencing increased vulnerability with changing climate or in other words with VI < 0 could be either due to changes in  $\Delta P$  or  $\Delta PET$  or both. Instances of VI < 0 but positive  $\Delta P$  indicate that changes in precipitation do not contribute to increased vulnerability in these basins. Conversely, for basins with VI < 0 but with negative  $\Delta PET$ , it can be concluded that only reductions in precipitation is the cause for vulnerability. For the basins where both changes in P and PET contribute to VI < 0, we can quantify the relative contribution of these variables on VI. To this end,  $\Delta WA$  or the numerator of the right hand side of Equation 4 is rewritten as:

$$\Delta WA = \frac{\partial WA}{\partial P} \triangle P + \frac{\partial WA}{\partial PET} \triangle PET$$
 (5)

The contribution of  $\Delta P$  and  $\Delta PET$  to  $\Delta WA$  is given by the first and second terms, respectively, of the right hand side of Equation 5. Using Equations 1–3,  $\frac{\partial WA}{\partial P}$  and  $\frac{\partial WA}{\partial PET}$  can be derived as (Table S2 in Supporting Information S1)

$$\frac{\partial WA}{\partial P} = \frac{\partial \left(Px^{\frac{1}{\omega}} - PET\right)}{\partial P} \text{ and } \frac{\partial WA}{\partial PET} = \frac{\partial \left(Px^{\frac{1}{\omega}} - PET\right)}{\partial PET}$$
 where  $x = \left(1 + \left(\frac{PET}{P}\right)^{\omega}\right)$ 

After partial differentiation, the above terms reduce to

$$\frac{\partial WA}{\partial P} = \left(\frac{-PET^{\omega}}{P^{\omega}}\right) \left(\frac{x_i}{x_i} \frac{1}{\omega}\right) + x_i^{\frac{1}{\omega}}$$
(6)

$$\frac{\partial WA}{\partial PET} = \frac{P}{PET} \left( \frac{PET^{\omega}}{P^{\omega}} \right) \left( \frac{x_i}{x_i}^{\frac{1}{\omega}} \right) - 1$$
 (7)

WOLKEBA ET AL. 3 of 10

The relative contributions (RCs) of changes in P and PET to increased vulnerability or VI < 0 can now be calculated as:

$$RC[\Delta P] = \frac{\frac{\partial WA}{\partial P}}{\Delta WA} \frac{\Delta P}{\Delta WA} \text{ and } RC[\Delta PET] = \frac{\frac{\partial WA}{\partial PET}}{\Delta WA} \frac{\Delta PET}{\Delta WA}$$
(8)

Equations 5–8 indicate that the relative contributions of  $\Delta P$  and  $\Delta PET$  in the different aridity zones depend on the projected changes in P, PET, and the prevailing hydroclimateology in the basins.

#### 3. Study Area and Data Used

The study is conducted in 331 out of 335 HUC06 basins in the CONUS. Four HUC06 basins, viz., Ventura-San Gabriel Coastal (HUC06 code = 180701), Upper South Saskatchewan River (HUC06 code = 090400), Onslow Bay (HUC06 code = 030203) and Mid Atlantic Coastal (HUC06 code = 020403), are left out from the analysis due to boundary issues related to zonal statistics computations. Except for the Lower Mississippi-Baton Rouge basin (HUC06 code = 080701), all basins in HUC06 have an area greater than 1,000 Km<sup>2</sup>.

Precipitation (P), evapotranspiration (ET), and potential evapotranspiration (PET) data are used in the ensuing analysis. A 20-year analysis period (also called the base period, hereafter) from 2001 to 2020, is used for generation of Budyko curve for each river basin. Precipitation is extracted from NLDAS-2 data set. NLDAS-2 provides estimates of climatological properties by combining data from multiple sources of observations and reanalysis (Xia et al., 2012). ET and PET are extracted from MODIS Version 6 Evapotranspiration/Latent Heat Flux product (Running et al., 2021). MODIS gives estimates of ET and PET using Penman-Monteith equation and remotely sensed data. The ET from MODIS has been previously validated using observations at eddy covariance flux towers (Running et al., 2021). The gridded hourly NLDAS-2 and the 8-day MODIS (ET and PET) data are aggregated to annual values per grid. These annual values are then averaged over HUC06 basins to estimate annual basin values using google earth engine.

To assess the impacts on water availability in a future climate, projected precipitation and other climate variables from five climate models of the sixth phase of Coupled Model Intercomparison Project (CMIP6) for 2015–2034 and 2081–2100 are used. We use an ensemble of models as the climate projections may vary depending on the climate model used. In this regard, Climate models from Geophysical Fluid Dynamics Laboratory (GFDL), Institut Pierre Simon Laplace (IPSL), Max Planck Institute (MPI), Meteorological Research Institute (MRI) and UK Earth System Model (UKESM) are used in this study. The projected climate data is obtained from the ISIMIP data portal (ISIMIP3b, 2022). The data sets are bias-corrected and statistically downscaled. Two future scenarios from the climate models are used, the higher CO<sub>2</sub> emission scenario, SSP585, and the lower emission scenario, SSP126. Scenario SSP585 is an update of RCP8.5 while SSP126 is an optimistic remake of RCP2.6. More details regarding the concerned data, including their spatio-temporal resolution are listed in Table S1 in Supporting Information S1. PET for the two periods (2015–2034 and 2081–2100) is calculated using the Community Water Model (CWatM) (Burek et al., 2020), an open-source global hydrological model that uses the Penman-Monteith method (Allen et al., 1998) to estimate PET. PET is calculated independently using climate data from five different models and for both scenarios.

#### 4. Results and Discussions

#### 4.1. Effectiveness of Fitted Budyko Curves for ET Estimation

Fu's parameter,  $\omega$  (see Equation 1), is calibrated to minimize RMSE between Budyko estimated evapotranspiration and evapotranspiration from MODIS. For the base period (2001–2020), the average RMSE over all selected HUC06 basins in the CONUS is 0.074. The RMSE distribution in Figure S1 in Supporting Information S1 shows the goodness of fit of derived  $\omega$  in the basins. Notably, coastal areas such as Salton Sea, San Francisco Bay and Central California have large RMSE (Figure S1 in Supporting Information S1). It could be due to extreme droughts during the base period (Maurer et al., 2022). Expectedly,  $\omega$  shows significant spatial variations over the US (Figure S2 in Supporting Information S1) with values ranging from 1.1 to 3 (Figure S3 in Supporting Information S1). The estimated median  $\omega$  value over the HUC06 basins is 1.68 with a mean of 1.67.

To assess the representativeness of  $\omega$ , respective long-term ET estimates for each basin are plotted against MODIS estimates (Figure S6 in Supporting Information S1). Fitted  $\omega$  values for each basin result in close correlation with

WOLKEBA ET AL. 4 of 10

19448007, 2023, 24, Downloaded from https://agupubs.onlinelibrary.wiley.com/doi/10.1029/2023GL/106004, Wiley Online Library on [13/01/2024]. See the Terms and Conditions (https://onlinelibrary.wiley.com/terms-and-conditions) on Wiley Online Library for rules of use; OA articles are governed by the applicable Creative Commons Licensia.

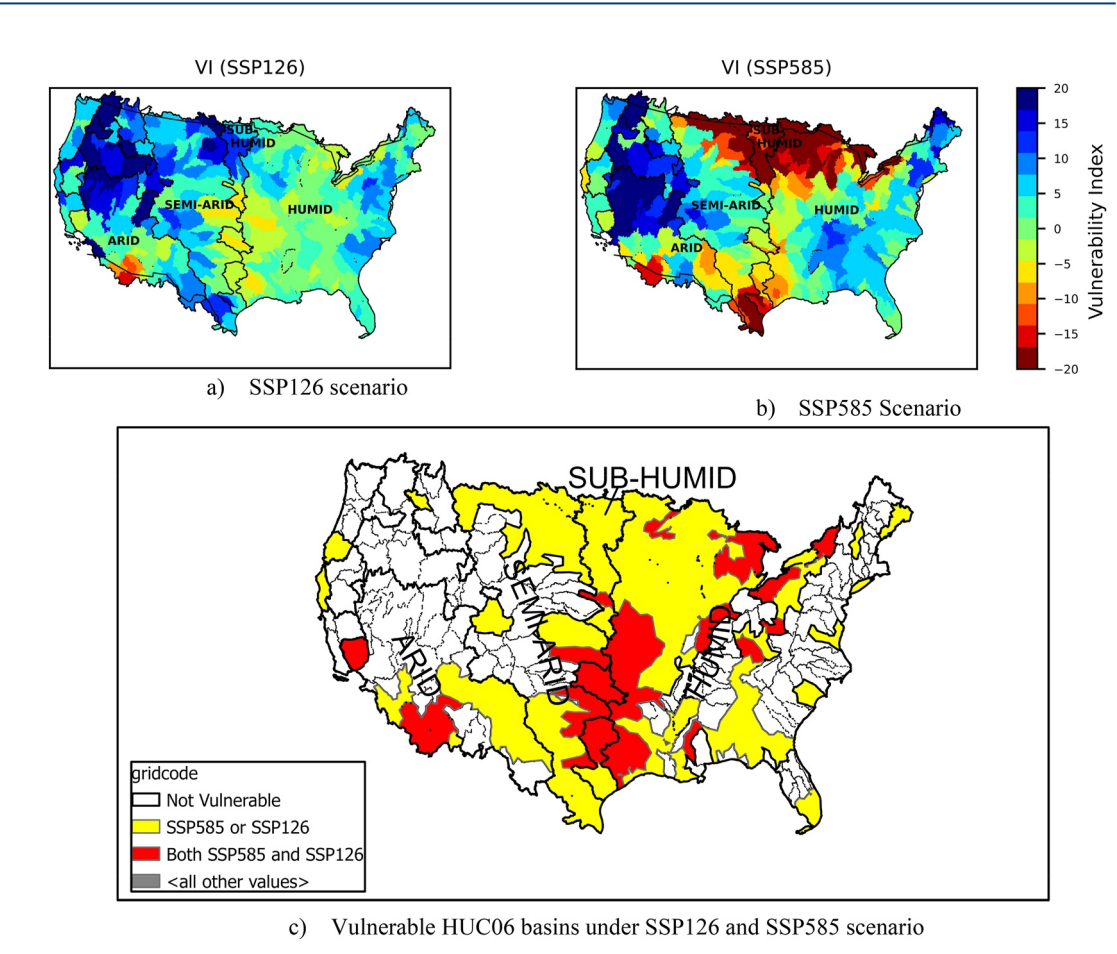


Figure 1. Spatial distribution of vulnerability index in (a) SSP126, and (b) SSP585 scenarios. (c) Map of vulnerable basins under SSP126 and SSP585 scenarios.

the MODIS ET data set. Notably, ET estimates based on the median  $\omega = 1.68$  and the default Budyko  $\omega = 2.6$  show large discrepancies from the MODIS actual ET values. The results highlight that using single  $\omega$  across all basins may have a substantial impact on ET estimation, and consequently assessment of water availability, as has been also reported by many previous studies (Greve et al., 2015; Gunkel & Lange, 2017; Guo et al., 2019; Koppa et al., 2021; Singh & Kumar, 2015; Wang & Tang, 2014; Xu et al., 2013; Yao et al., 2020).

#### 4.2. Hydroclimatological Classification of Selected Basins

Here we use a (Middleton & Thomas, 1992) classification based on aridity index (AI), which is the ratio of potential evapotranspiration and precipitation. AI  $\leq$  1.5, 1.5 < AI  $\leq$  2, 2 < AI  $\leq$  5, and AI > 5 correspond to humid, sub-humid, semi-arid, and arid regions. Among the 331 basins, 187 are humid, 28 are sub-humid, 75 are semi-arid, and 41 are arid. We estimate AI of each basin for both SSP585 and SSP126 scenarios and find that 88.22% and 96.37% of basins, respectively, remain in their current aridity zone classification (Figure S4 in Supporting Information S1). The Fu's parameter shows contrasts for basins failing within distinct hydroclimatic classifications (Figure S5 in Supporting Information S1).

#### 4.3. Vulnerability of Water Availability With Changing Climate

The impact of changing climate on water availability is tracked using the vulnerability index (VI), as estimated using Equation 4. Results show significant spatial heterogeneity in VI across basins (Figure 1). VI also varies between scenarios and between climate models (Figures S7 and S10 in Supporting Information S1). For ensuing analyses, the median VI is first evaluated for each basin. Most HUC06 basins in the Northwest, West, Ohio Valley and Northeast show minimal vulnerability. Basins such as Arkansas-Keystone, Lower Cimarron, Lower North

WOLKEBA ET AL. 5 of 10

**Table 1**Causes of Vulnerability Under SSP126 and SSP585 Scenarios

Zone	Number of vulnerable basins in SSP126 scenario	Number of vulnerable basins in SSP585 scenario	Cause of vulnerability VI < 0
Humid	63 (33.7%)	78 (41.7%)	23 in SSP126 and 71 in SSP585 as a result of PET. This is equivalent to 37% and 91% of the basins with VI < 0 in the respective scenarios. Remaining basins have VI < 0 as a result of changes in both P and PET.
Sub Humid	10 (35.7%)	19 (67.9%)	1 in SSP126 and 10 in SSP585 have VI < 0 contributed by PET. Remaining basins experience VI < 0 due to changes in both P and PET.
Semi-Arid	10 (13.3%)	30 (40.0%)	In SSP126, there are 2 basins out of 10 (=20%) where VI < 0 is a result of PET. Likewise, in SSP585, there are 14 basins out of 30 (=47%) where VI < 0 is attributed to PET. For the remaining basins in both scenarios, VI < 0 occurs due to changes in both precipitation (P) and potential evapotranspiration (PET).
Arid	10 (24.4%)	15 (36.6%)	4 in SSP585 has VI < 0 as a result of PET. Remaining basins experience VI < 0 due to changes in both P and PET.

Canadian, Lower Canadian, Verdigris, and Missouri-Nishnabotna are vulnerable in both SSP126 and SSP585 scenarios. There are also basins, such as Rio Grande-Amistad basin, that are vulnerable only in the SSP126 scenario. On the other hand, basins in the Upper Midwest, Western Ohio Valley, and Southern US show relatively high vulnerability to climate change in the higher emission scenario. This is largely attributable to an increase in PET in the Upper Midwest US and the combined effect of reduced precipitation and increased PET in the Southern US (Figure S11 in Supporting Information S1). Alarmingly, some basins in arid regions, such as Santa Cruz in Arizona, are projected to have lower water availability, exacerbating the prevailing dry conditions in the basins. Most arid basins in the West (Northwest, Southwest, and West North Central) are predicted to have an increase in water availability in 2081–2100 in both SSP126 and SSP585 scenarios. Notably, the overall spatial distribution of VI is similar even when it is evaluated as the mean across climate models for each river basin (Figures S12 to S14 in Supporting Information S1).

The box plots (Figure S8 in Supporting Information S1) of VI in different aridity zones show that most of the humid and arid basins are not under water stress due to climate change, as the median VI for most of these basins are greater than zero in both the SSP126 and SSP585 scenarios. On the other hand, most sub-humid and semi-arid basins are vulnerable under the SSP585 scenario. Overall, the results show that fewer basins are affected by water scarcity under the SSP126 scenario. The SSP585 scenario, on the other hand, predicts less water availability in most sub-humid and semi-arid basins. In the SSP585 scenario a larger fraction of sub-humid and semi-arid basins are vulnerable (Table 1), however, there are also a large number of vulnerable humid basins overall.

#### 4.4. Parsing the Relative Controls on Water Vulnerability With Changing Climate

Scatter plots of median VI across climate models (GFDL, IPSL, MPI, MRI, and UKESM) for each basin, lying in different aridity zones is drawn (Figure 2) to assess how basins' vulnerability is affected by the projected changes in P and PET. The median of VI,  $\Delta P$ , and  $\Delta PET$  over all basins is calculated for both SSP126 and SSP585 scenarios. The blue colors show VI > 0%, the yellow colors show -10% < VI < 0%, and the red colors show VI < -10%. Circles indicate the SSP126 scenario, and triangles indicate the SSP585 scenario. Figure 2 shows that in many instances of VI < 0%,  $\Delta P$  is positive thus indicating that changes in precipitation do not contribute to increased vulnerability in these basins. Further parsing of  $\Delta P$  and  $\Delta PET$  for all basins with VI < 0% indicate that there are no basins becoming vulnerable solely as a result of reduced P. Table 1 summarizes the causes for vulnerability of basins in the different aridity zone classes. 28% and 70% of the total vulnerable basins in SSP126 and SSP585 scenarios, respectively, experience increased vulnerability only due to increase in PET. Similarly, 72% and 30% of the total vulnerable basins in SSP126 and SSP585 scenarios, respectively, experience increased vulnerability due to both an increase in PET and a decrease in P with changing climate. These results indicate that instances of increased vulnerability solely due to the contribution of increase in PET is more frequent for the higher CO<sub>2</sub> emission scenario (or SSP585). For the SSP585 scenario, a majority of the basins in humid and arid regions with VI < 0% experience such solely due to contribution of positive  $\Delta PET$ . Overall, among the basins

WOLKEBA ET AL. 6 of 10

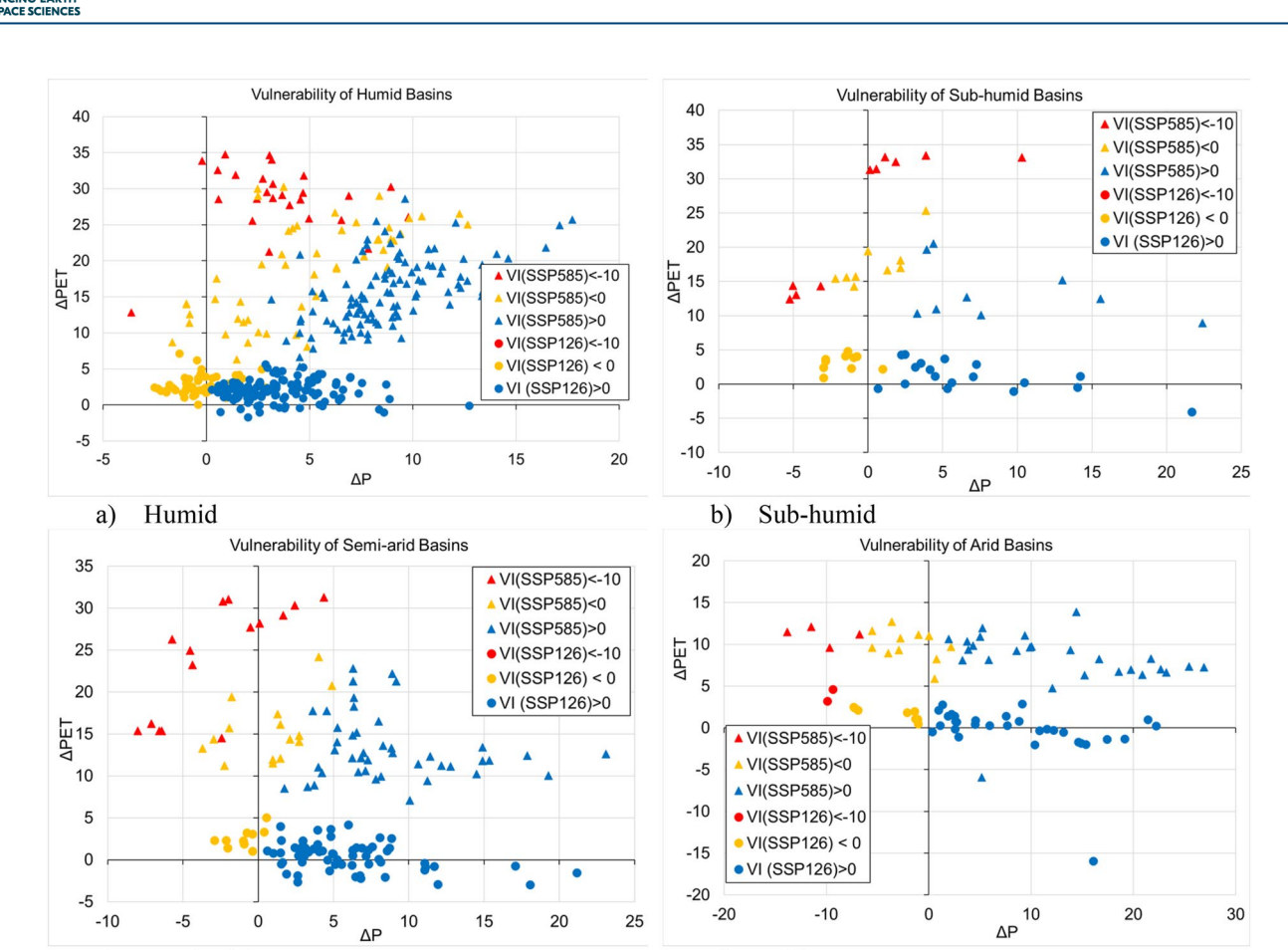


Figure 2. Vulnerability index values in HUC06 basins in the CONUS (a) humid, (b) sub-humid, (c) semi-arid and (d) arid basins.

c)

Semi-arid

experiencing increase in vulnerability with changing climate, humid basins experience a higher contribution of  $\Delta PET$  more often than others.

d)

Arid

For the basins where both changes in P and PET contribute to VI < 0, we quantify the relative contributions of both  $\Delta P$  and  $\Delta PET$  to VI using Equation 8. Histogram plots of the two contributions are shown in Figure 3 and Figure S9 in Supporting Information S1. The plots show that the relative contribution of PET in these basins is generally larger than that of P in SSP585 scenario, except in arid settings. However, in the SSP126 scenario, the relative dominance of  $\Delta P$  to vulnerability is generally more prevalent except in humid settings.

#### 5. Conclusions and Synthesis

The study maps the changes in long-term water availability due to projected climate change under a low-emission (SSP126) and a higher-emission (SSP585) scenarios. This was achieved by integrating climate predictions in the Budyko framework to assess changes in water availability in HUC06 basins over the CONUS. These predictions are then used to assess the vulnerability of HUC06 basins, in different aridity settings. Finally, the study evaluates the relative role of changes in precipitation and potential evapotranspiration on vulnerability of basins. Results show that 28.10% and 42.90% of basins are projected to experience increased vulnerability (i.e., VI < 0%) in low-(SSP126) and high- (SSP585) emission scenarios, respectively. Sub-humid basins are projected to most often experience increase in vulnerability in both the considered scenarios. We also find that among the vulnerable basins, 69.72% and 27.96% of them are affected only by an increase in potential evapotranspiration in SSP585 and SSP126 scenarios, respectively, while the remaining vulnerable basins are affected by both an increase in potential evapotranspiration and a decrease in precipitation. The relative contribution of potential evapotranspiration to vulnerability is greater than precipitation in all basins in higher emission scenarios, except in arid

WOLKEBA ET AL. 7 of 10

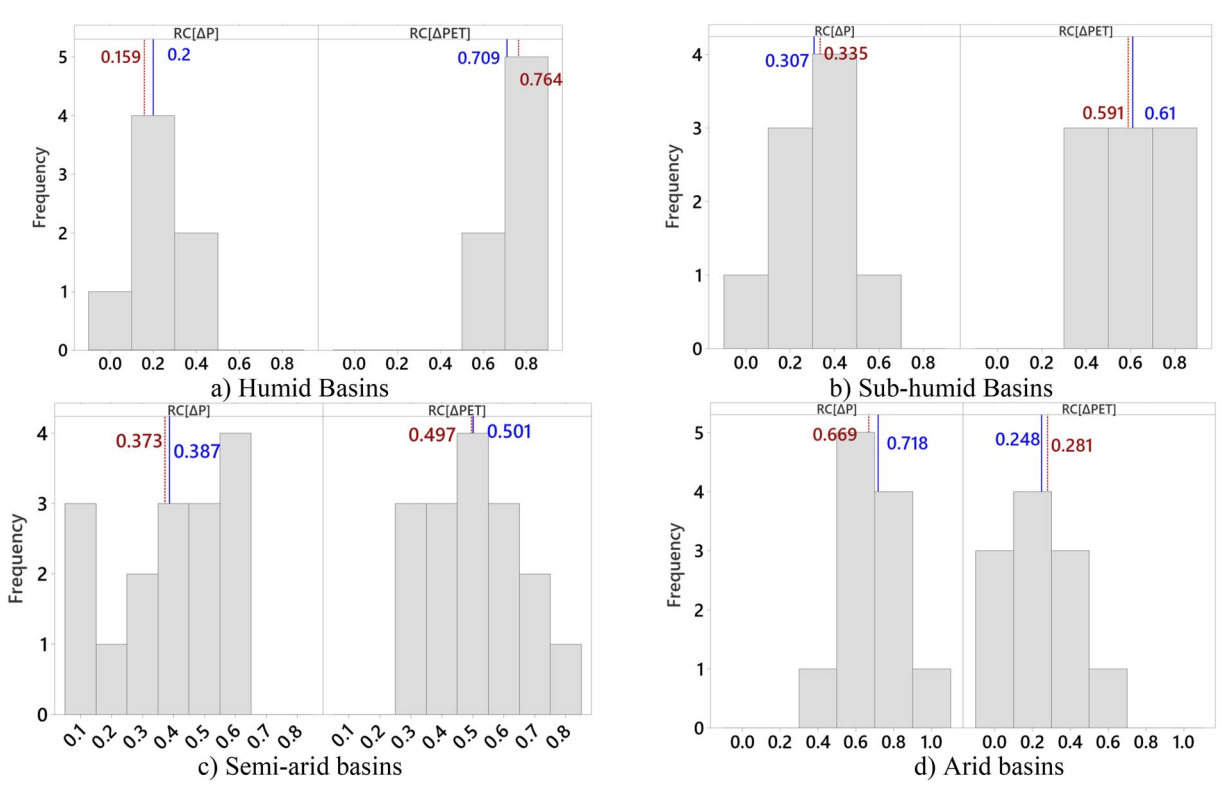


Figure 3. Relative contributions (RCs) of P and PET in (a) humid, (b) sub-humid, (c) semi-arid and (d) arid basins, experiencing VI < 0 in the SSP585 scenario. Note the selected basins are the ones where both  $\Delta P$  and  $\Delta PET$  contribute to increase in vulnerability. The blue solid line indicates the mean value and the red dashed line is the median.

settings. However, in the lower emission scenario, that is, the SSP126, the relative dominance of  $\Delta P$  to vulnerability is generally more prevalent except in humid settings. None of the basins are projected to experience a vulnerability increase only due to reduction in precipitation. If we use the averaged projected population data of 464.495 million people for 2081–2099 from (ISIMIP2b, 2022), it is estimated that the number of people that will be exposed to the projected vulnerability will be around 98.09 and 183.5 million people in SSP126 and SSP585 scenarios, respectively.

It is to be noted that there are many sources of uncertainty when predicting future changes in water availability, and consequent vulnerability of river basins. For example, available data for model definition may not be representative, and climate projections may have uncertainties. Land use and other anthropogenic changes will also affect water availability. In addition to sharing these limitations, the Budyko framework used in this study does not consider water abstractions other than evaporation. Such effort would require the challenging task of dynamic modeling of Budyko parameters (Li & Quiring, 2022), which can introduce additional uncertainty in analysis. Recent studies question Budyko curve validity over time, especially for the future (Jaramillo et al., 2022; Reaver et al., 2022). These discrepancies may stem from climate models' inability to account for vegetation-climate co-evolution. The data in some watersheds may not fit the Budyko curve due to the absence of natural vegetation-water co-evolution as well, driven largely by human activity. Timescale differences between vegetation response to climate changes may also impact the Budyko curve's validity for considered analysis times. Further studies are needed to fully understand Budyko curve limitations as a function of natural vegetation-water-energy co-evolution. It was assumed that there is no significant effect of climate change on land use change or on climate seasonality and storminess in the basins for the purpose of simulating water availability changes due to climate change alone. Another limitation of this study is that the results depend on the input data used. Moreover, the vulnerability index used in this study only accounts for larger time-step budgetary changes and does not account for water scarcity induced vulnerability at a finer temporal resolution.

Despite these inherent uncertainties and limitations, this study shows that Budyko curves can be used to estimate the vulnerability of future water availability with changes in climate. The study presents a novel methodology

WOLKEBA ET AL. 8 of 10

19448007, 2023, 24, Downloaded from https://agupubs.onlinelibrary.wiley.com/doi/10.1029/2023GL106004, Wiley Online Library on [13/01/2024]. See the Terms and Conditions

Acknowledgments

This work was supported by the Global

Water Security Center (GWSC), Alabama

Water Institute. M.K. also acknowledges

partial support of National Science

EAR-1856054, and DGE-2152140.

Foundation grants OIA-2019561,

to assess whether the changes in precipitation or potential evapotranspiration is the main driver of future water vulnerability, and uses it to quantify their individual contributions. As the results show that a sizeable population is projected to experience water vulnerability in future climate, the study underscores the urgent need to devise long-term solutions to mitigate projected vulnerability of water availability in affected basins.

#### **Conflict of Interest**

The authors declare no conflicts of interest relevant to this study.

#### **Data Availability Statement**

Data is available at Wolkeba et al. (2023).

#### References

Abatzoglou, J. T. (2013). Development of gridded surface meteorological data for ecological applications and modelling. *International Journal of Climatology*, 33(1), 121–131. https://doi.org/10.1002/joc.3413

Abera, W., Tamene, L., Abegaz, A., & Solomon, D. (2019). Understanding climate and land surface changes impact on water resources using Budyko framework and remote sensing data in Ethiopia. *Journal of Arid Environments*, 167, 56–64. https://doi.org/10.1016/j.iaridenv.2019.04.017

Allen, R. G., Pereira Luis, S., Dirk, R., & Martin, S. (1998). Crop evapotranspiration - Guidelines for computing crop water requirements - FAO Irrigation and drainage paper 56. FAO.

Berelson, W. L., Caffrey, P. A., & Hamerlinck, J. D. (2004). Mapping hydrologic units for the national watershed boundary dataset. *Journal of the American Water Resources Association*, 40(5), 1231–1246. https://doi.org/10.1111/j.1752-1688.2004.tb01582.x

Berghuijs, W. R., Larsen, J. R., van Emmerik, T. H. M., & Woods, R. A. (2017). A global assessment of runoff sensitivity to changes in precipitation, potential evaporation, and other factors. Water Resources Research, 53(10), 8475–8486. https://doi.org/10.1002/2017wr021593

Bouaziz, L. J. E., Aalbers, E. E., Weerts, A. H., Hegnauer, M., Buiteveld, H., Lammersen, R., et al. (2022). Ecosystem adaptation to climate change: The sensitivity of hydrological predictions to time-dynamic model parameters. *Hydrology and Earth System Sciences*, 26(5), 1295–1318. https://doi.org/10.5194/hess-26-1295-2022

Budyko, M. I. (1961). The heat balance of the Earth's surface. *Soviet Geography*, 2(4), 3–13. https://doi.org/10.1080/00385417.1961.10770761 Burek, P., Satoh, Y., Kahil, T., Tang, T., Greve, P., Smilovic, M., et al. (2020). Development of the community water model (CWatM v1.04) - A

Burek, P., Satoh, Y., Kahil, T., Tang, T., Greve, P., Smilovic, M., et al. (2020). Development of the community water model (CWatM v1.04) - A high-resolution hydrological model for global and regional assessment of integrated water resources management. Geoscientific Model Development, 13(7), 3267–3298. https://doi.org/10.5194/gmd-13-3267-2020

Carmona, A. M., Sivapalan, M., Yaeger, M. A., & Poveda, G. (2014). Regional patterns of interannual variability of catchment water balances across the continental US: A Budyko framework. Water Resources Research, 50(12), 9177–9193. https://doi.org/10.1002/2014wr016013

EU. (2015). Guidance Document No. 34. Guidance document on the application of water balances for supporting the implementation of the WFD (Vol. 10)

Fisher, R. A., Koven, C. D., Anderegg, W. R. L., Christoffersen, B. O., Dietze, M. C., Farrior, C. E., et al. (2018). Vegetation demographics in Earth system models: A review of progress and priorities. *Global Change Biology*, 24(1), 35–54. https://doi.org/10.1111/gcb.13910

Fu, B. P. (1981). On the calculation of the evaporation from land surface (in Chinese). Scientia Atmospherica Sinica, 5, 23–31.

Gan, G. J., Liu, Y. B., & Sun, G. (2021). Understanding interactions among climate, water, and vegetation with the Budyko framework. Earth-Science Reviews, 212, 103451. https://doi.org/10.1016/j.earscirev.2020.103451

Greve, P., Gudmundsson, L., Orlowsky, B., & Seneviratne, S. I. (2015). Introducing a probabilistic Budyko framework. Geophysical Research Letters, 42(7), 2261–2269. https://doi.org/10.1002/2015g1063449

Greve, P., Gudmundsson, L., & Seneviratne, S. I. (2018). Regional scaling of annual mean precipitation and water availability with global temperature change. Earth System Dynamics, 9(1), 227–240. https://doi.org/10.5194/esd-9-227-2018

Guan, X. X., Zhang, J. Y., Bao, Z. X., Liu, C. S., Jin, J. L., & Wang, G. Q. (2021). Past variations and future projection of runoff in typical basins in 10 water zones, China. Science of the Total Environment, 798, 149277. https://doi.org/10.1016/j.scitotenv.2021.149277

Guan, X. X., Zhang, J. Y., Yang, Q. L., & Wang, G. Q. (2022). Quantifying the effects of climate and watershed structure changes on runoff variations in the Tao River basin by using three different methods under the Budyko framework. *Theoretical and Applied Climatology*, 151(3–4), 953–966. https://doi.org/10.1007/s00704-021-03894-5

Gudmundsson, L., Greve, P., & Seneviratne, S. I. (2016). The sensitivity of water availability to changes in the aridity index and other factors-A probabilistic analysis in the Budyko space. *Geophysical Research Letters*, 43(13), 6985–6994. https://doi.org/10.1002/2016gl069763

Gunkel, A., & Lange, J. (2017). Water scarcity, data scarcity and the Budyko curve-An application in the Lower Jordan River Basin. Journal of Hydrology-Regional Studies, 12, 136–149. https://doi.org/10.1016/j.ejrh.2017.04.004

Guo, A. J., Chang, J. X., Wang, Y. M., Huang, Q., Guo, Z. H., & Li, Y. Y. (2019). Uncertainty analysis of water availability assessment through the Budyko framework. *Journal of Hydrology*, 576, 396–407. https://doi.org/10.1016/j.jhydrol.2019.06.033

ISIMIP2b. (2022). Population ssp2soc 2006-2099 [Dataset]. ISIMIP. Retrieved from https://files.isimip.org/ISIMIP2b/InputData/population/rcp26soc/

ISIMIP3b. (2022). ISIMIP3b bias-adjusted atmospheric climate input data Version 1.1 [Dataset]. ISIMIP3b. https://doi.org/10.48364/ ISIMIP.842396.1

Jaramillo, F., Piemontese, L., Berghuijs, W. R., Wang-Erlandsson, L., Greve, P., & Wang, Z. Q. (2022). Fewer basins will follow their Budyko curves under global warming and fossil-fueled development. Water Resources Research, 58(8), e2021WR031825. https://doi. org/10.1029/2021WR031825

Kollet, S. J., & Maxwell, R. M. (2006). Integrated surface-groundwater flow modeling: A free-surface overland flow boundary condition in a parallel groundwater flow model. Advances in Water Resources, 29(7), 945–958. https://doi.org/10.1016/j.advwatres.2005.08.006

Konapala, G., Mishra, A. K., Wada, Y., & Mann, M. E. (2020). Climate change will affect global water availability through compounding changes in seasonal precipitation and evaporation. *Nature Communications*, 11(1), 3044. https://doi.org/10.1038/s41467-020-16757-w

WOLKEBA ET AL. 9 of 10

- Koppa, A., Alam, S., Miralles, D. G., & Gebremichael, M. (2021). Budyko-based long-term water and energy balance closure in global water-sheds from Earth observations. Water Resources Research, 57(5), e2020WR028658. https://doi.org/10.1029/2020WR028658
- Koutroulis, A. G., Papadimitriou, L. V., Grillakis, M. G., Tsanis, I. K., Warren, R., & Betts, R. A. (2019). Global water availability under high-end climate change: A vulnerability based assessment. Global and Planetary Change, 175, 52–63. https://doi.org/10.1016/j.gloplacha.2019.01.013
- Koyen, C. D., Knox, R. G., Fisher, R. A., Chambers, J. Q., Christoffersen, B. O., Davies, S. J., et al. (2020). Benchmarking and parameter sensitivity of physiological and vegetation dynamics using the functionally assembled terrestrial ecosystem simulator (FATES) at Barro Colorado Island, Panama. *Biogeosciences*, 17(11), 3017–3044. https://doi.org/10.5194/bg-17-3017-2020
- Kumar, M., Duffy, C. J., & Salvage, K. M. (2009). A second-order accurate, finite volume-based, integrated hydrologic modeling (FIHM) framework for simulation of surface and subsurface flow. *Vadose Zone Journal*, 8(4), 873–890. https://doi.org/10.2136/vzj2009.0014
- Li, Z. Y., & Quiring, S. M. (2022). Projection of Streamflow change using a time-Varying Budyko framework in the contiguous United States. Water Resources Research, 58(10), e2022WR033016. https://doi.org/10.1029/2022WR033016
- Martens, C., Hickler, T., Davis-Reddy, C., Engelbrecht, F., Higgins, S. I., von Maltitz, G. P., et al. (2021). Large uncertainties in future biome changes in Africa call for flexible climate adaptation strategies. Global Change Biology, 27(2), 340–358. https://doi.org/10.1111/gcb.15390
- Maurer, T., Avanzi, F., Glaser, S. D., & Bales, R. C. (2022). Drivers of drought-induced shifts in the water balance through a Budyko approach. Hydrology and Earth System Sciences, 26(3), 589–607. https://doi.org/10.5194/hess-26-589-2022
- Mekonnen, M. M., & Hoekstra, A. Y. (2016). Four billion people facing severe water scarcity. Science Advances, 2(2), e1500323. https://doi.org/10.1126/sciadv.1500323
- Middleton, N., & Thomas, D. (1992). World atlas of desertification. Edward Arnold.
- Pike, J. G. (1964). The estimation of annual runoff from meteorological data in a tropical climate. *Journal of Hydrology*, 2, 116–123. https://doi.org/10.1016/0022-1694(64)90022-8
- Pokhrel, Y., Felfelani, F., Satoh, Y., Boulange, J., Burek, P., Gadeke, A., et al. (2021). Global terrestrial water storage and drought severity under climate change. Nature Climate Change, 11(3), 226–233. https://doi.org/10.1038/s41558-020-00972-w
- Ravazzani, G., Barbero, S., Salandin, A., Senatore, A., & Mancini, M. (2015). An integrated hydrological model for assessing climate change impacts on water resources of the upper Po River Basin. Water Resources Management, 29(4), 1193–1215. https://doi.org/10.1007/ s11269-014-0868-8
- Reaver, N. G. F., Kaplan, D. A., Klammler, H., & Jawitz, J. W. (2022). Theoretical and empirical evidence against the Budyko catchment trajectory conjecture. Hydrology and Earth System Sciences, 26(5), 1507–1525. https://doi.org/10.5194/hess-26-1507-2022
- Running, S., Mu, Q., & Zhao, M. (2021). MOD16A2 MODIS/Terra net evapotranspiration 8-day L4 global 500m SIN grid V006.2017, distributed by NASA EOSDIS land processes DAAC. https://doi.org/10.5067/MODIS/MOD16A2.006
- Schreiber, P. (1904). U" ber die Beziehungen zwischen dem Niederschlag und der Wasserfu"hrung der Flu"ße in Mitteleuropa. Zeitschrift für Meteorologie. 21, 441–452.
- Singh, R., & Kumar, R. (2015). Vulnerability of water availability in India due to climate change: A bottom-up probabilistic Budyko analysis. Geophysical Research Letters, 42(22), 9799–9807. https://doi.org/10.1002/2015gl066363
- Telteu, C. E., Schmied, H. M., Thiery, W., Leng, G. Y., Burek, P., Liu, X. C., et al. (2021). Understanding each other's models: An introduction and a standard representation of 16 global water models to support intercomparison, improvement, and communication. *Geoscientific Model Development*, 14(6), 3843–3878. https://doi.org/10.5194/gmd-14-3843-2021
- Teng, J., Chew, F. H. S., Vaze, J., Marvanek, S., & Kirono, D. G. C. (2012). Estimation of climate change impact on mean annual runoff across continental Australia using Budyko and Fu equations and hydrological models. *Journal of Hydrometeorology*, 13(3), 1094–1106. https://doi.org/10.1175/Jhm-D-11-097.1
- Teshome, F., Moges, S. A., & Hailu, D. (2019). Chapter 14 Evaluation of globally available water resources reanalysis (WRR-1) runoff products for assessment and management water resources in the Upper Blue Nile basin: A data scarce major subbasins of the Nile basin. In A. M. Melesse, W. Abtew, & G. Senay (Eds.), *Extreme hydrology and climate variability* (pp. 165–173). Elsevier. https://doi.org/10.1016/B978-0-12-815998-9.00014-2
- VanderKwaak, J. E., & Loague, K. (2001). Hydrologic-response simulations for the R-5 catchment with a comprehensive physics-based model. Water Resources Research, 37(4), 999–1013. https://doi.org/10.1029/2000wr900272
- Viola, F., Caracciolo, D., & Deidda, R. (2021). Modelling the mutual interactions between hydrology, society and water supply systems. *Hydrological Sciences Journal-Journal Des Sciences Hydrologiques*, 66(8), 1265–1274. https://doi.org/10.1080/02626667.2021.1909729
- Wang, D. B., & Hejazi, M. (2011). Quantifying the relative contribution of the climate and direct human impacts on mean annual streamflow in the contiguous United States. Water Resources Research, 47(10), W00j12. https://doi.org/10.1029/2010wr010283
- Wang, D. B., & Tang, Y. (2014). A one-parameter Budyko model for water balance captures emergent behavior in darwinian hydrologic models. Geophysical Research Letters, 41(13), 4569–4577. https://doi.org/10.1002/2014g1060509
- Weiskel, P. K., Vogel, R. M., Steeves, P. A., Zarriello, P. J., DeSimone, L. A., & Ries, K. G. (2007). Water use regimes: Characterizing direct human interaction with hydrologic systems. Water Resources Research, 43(4), W04402. https://doi.org/10.1029/2006wr005062
- Wolkeba, F., Kumar, M., & Mekonnen, M. (2023). Examining the water scarcity vulnerability in US river basins due to changing climate [Dataset]. HydroShare. http://www.hydroshare.org/resource/3baebff452a84a8c82fe62d7dd82bc37
- Xia, Y. L., Mitchell, K., Ek, M., Sheffield, J., Cosgrove, B., Wood, E., et al. (2012). Continental-scale water and energy flux analysis and validation for the North American land data assimilation system project phase 2 (NLDAS-2): 1. Intercomparison and application of model products. Journal of Geophysical Research, 117(D3), D03109. https://doi.org/10.1029/2011jd016048
- Xu, X., Yang, D., Yang, H., & Lei, H. (2014). Attribution analysis based on the Budyko hypothesis for detecting the dominant cause of runoff decline in Haihe basin. *Journal of Hydrology*, 510, 530–540. https://doi.org/10.1016/j.jhydrol.2013.12.052
- Xu, X. L., Liu, W., Scanlon, B. R., Zhang, L., & Pan, M. (2013). Local and global factors controlling water-energy balances within the Budyko framework. Geophysical Research Letters, 40(23), 6123–6129. https://doi.org/10.1002/2013gl058324
- Yao, L. L., Libera, D. A., Kheimi, M., Sankarasubramanian, A., & Wang, D. B. (2020). The roles of climate forcing and its variability on streamflow at daily, monthly, annual, and long-term scales. Water Resources Research, 56(7), e2020WR027111. https://doi.org/10.1029/2020WR027111
- Zhang, L., DWalker, W. R. G. R., & Walker, G. R. (2001). Response of mean annual evapotranspiration to vegetation changes at catchment scale. Water Resources Research, 37(3), 701–708. https://doi.org/10.1029/2000wr900325
- Zhang, L., Hickel, K., Dawes, W. R., Chiew, F. H. S., Western, A. W., & Briggs, P. R. (2004). A rational function approach for estimating mean annual evapotranspiration. Water Resources Research, 40(2), W02502. https://doi.org/10.1029/2003wr002710

WOLKEBA ET AL. 10 of 10